The binding energy and structure of biexcitons in quantum wires

Li-Xue Zhai, Yan Wang, Wen-Dan Miao, and Jian-Jun Liu

Citation: Journal of Applied Physics **114**, 093702 (2013); doi: 10.1063/1.4819959
View online: http://dx.doi.org/10.1063/1.4819959
View Table of Contents: http://scitation.aip.org/content/aip/journal/jap/114/9?ver=pdfcov
Published by the AIP Publishing

The binding energy and structure of biexcitons in quantum wires

Li-Xue Zhai,[1] Yan Wang,[2] Wen-Dan Miao,[1] and Jian-Jun Liu[1,3,a)]
[1]*College of Physics & Information Engineering and Hebei Advanced Thin Film Laboratory, Hebei Normal University, Shijiazhuang 050024, People's Republic of China*
[2]*Hebei Chemical & Pharmaceutical College, Shijiazhuang 050026, People's Republic of China*
[3]*Physics Department, Shijiazhuang University, Shijiazhuang 050035, People's Republic of China*

(Received 3 May 2013; accepted 16 August 2013; published online 3 September 2013)

This paper describes the use of the finite difference method to study the binding energy and the structure of a biexciton in a model parabolic quantum wire (QWR). The biexciton binding energies calculated for different QWR widths are compared with recent experimental data and reasonable agreement is obtained. The conditional wave function of the biexciton has been investigated, and the structure of a biexciton in a QWR has been found to be similar to that of the H_2 molecule. The pair correlation functions for particles in bound biexcitons have also been calculated, and a clear picture for the particle configuration in a biexciton is established. Through the study of the average interparticle distance in a biexciton, we find that the individual excitons may retain their identity in bound biexcitons. © *2013 AIP Publishing LLC*. [http://dx.doi.org/10.1063/1.4819959]

I. INTRODUCTION

In recent years, semiconductor quantum wires (QWRs) have become the subject of considerable research effort because of their potential for device applications and their importance in fundamental physics research.[1–8,26,27] Recent experimental observations indicate that excitons, which are hydrogenlike bound states formed by photoexcited electron-hole pairs, are the predominant optical features in QWRs. Experimentally, if the photoexcitation is strong enough, the formation of biexcitons (bound states of pairs of excitons) becomes possible.[7] Since the first observation of biexcitons in quantum wells (QWs) reported by Miller *et al.*,[9] biexcitons in low-dimensional semiconductor systems have been extensively studied both theoretically[2,3,10–16] and experimentally.[4–8,17–20] Moreover, exciton-biexciton systems cannot only provide a model system for the implementation of elementary quantum computing operations[21] but also allow the realization of a potential source of strongly correlated photon pairs.[22,23] Therefore, biexcitons in nanostructures have attracted a sustained interest. The properties of biexcitons, such as their binding energies,[10,17] wave functions,[3] pair correlation functions (PCFs),[13] and localization,[8,11,28] have been studied.

The binding energy of a biexciton in a quasi-one-dimensional (Q1D) semiconductor system is expected to be enhanced compared to the binding energy in the bulk material due to the spatial confinement of the electrons and holes. Crottini *et al.*[4] report a direct observation of Q1D biexcitons in high quality V-shaped GaAs/GaAlAs QWRs, and the biexciton binding energy was measured to be 1.2 meV. Guillet *et al.*[5] found the biexciton binding energy to be equal to 1.5 meV by measuring the photoluminescence spectrum of a 5-nm thick V-shaped QWR. To the best of our knowledge, no theoretical work has been devoted to QWRs to explain these experimental data. Therefore, it is instructive to compare these experimental results with numerical simulations.

In a two-dimensional (2D) system, Singh *et al.* proposed a square structure for biexcitons,[10] which supposes that the opposite charges were situated at the opposite vertices of a square. Theoretical calculations performed by Usukura *et al.*,[14] however, do not support this assumption, and the structure of biexcitons in low-dimensional semiconductor systems is still under discussion. As for Q1D semiconductors, to our knowledge, there have been no systematic studies of the structure of biexcitons. Hence, it is interesting to explore the conditional wavefunctions, interparticle distances, and PCFs of biexcitons in QWRs.

Actually, the biexciton problem in the context of quantum wires is somewhat complex, and there have been relatively few theoretical studies of biexcitons in quantum wires.[2,3] Unlike excitons in QWRs, there are no standard theoretical models for biexcitons in QWRs.

In this paper, we present calculations of the binding energies and the structures of biexcitons in QWRs based on the finite difference method. The purpose of this work is to investigate the quantum confinement effects on the binding energies of biexcitons and to examine the structures of biexcitons in QWRs. The remainder of this paper is organized as follows. In Sec. II, we describe our theoretical model, and in Sec. III, we present and discuss our numerical results. We summarize our results and draw conclusions in Sec. IV.

II. MODEL

We consider a biexciton in a parabolic QWR, which is defined by a 2D parabolic and isotropic confinement potential. We have restricted our attention to the ground states of the biexciton systems in which the two electrons have opposite spins, as do the two holes. Using the effective mass approximation, a biexciton in a parabolic QWR can be described by the Hamiltonian

$$H_{XX} = H_{1X} + H_{2X} + V_C, \tag{1}$$

a)Electronic mail: liujj@mail.hebtu.edu.cn

with

$$H_{iX} = \sum_{j=e,h}\left(-\frac{\hbar^2}{2m_{ij}^*}\nabla_j^2 + \frac{1}{2}m_{ij}^*\omega_j^2\rho_{ij}^2\right) - \frac{e^2}{\varepsilon|\mathbf{r}_{ie}-\mathbf{r}_{ih}|} \quad (2)$$

and

$$V_C = \frac{e^2}{\varepsilon}\left(\frac{1}{|\mathbf{r}_{1e}-\mathbf{r}_{2e}|} + \frac{1}{|\mathbf{r}_{1h}-\mathbf{r}_{2h}|} - \frac{1}{|\mathbf{r}_{1e}-\mathbf{r}_{2h}|} - \frac{1}{|\mathbf{r}_{1h}-\mathbf{r}_{2e}|}\right),$$

where i ($i=1, 2$) indicates the first or second exciton, the index j ($j=e, h$) indicates whether the particle is an electron or a hole, m_{ij}^* is the effective mass of the particle j in the ith exciton. ω is the frequency of the parabolic confining potential in the xy plane that models the width of the QWR. ε is the dielectric constant of the QWR material and e is the electron charge. $\boldsymbol{\rho}_{ij}$ is the projection of $\mathbf{r}_{ij}$ onto the plane orthogonal to the wire axis, which is chosen as the z-axis. We assume the lateral confinement is sufficiently large to allow us to treat the system as a Q1D system, i.e., we can separate the contribution to the wave function along the QWR axis, from the contribution in the xy plane

$$\Psi(\mathbf{r}_{1e},\mathbf{r}_{2e},\mathbf{r}_{1h},\mathbf{r}_{2h}) = \psi_\perp(\boldsymbol{\rho}_{1e},\boldsymbol{\rho}_{2e},\boldsymbol{\rho}_{1h},\boldsymbol{\rho}_{2h}) \times \phi_{||}(z_{1e},z_{2e},z_{1h},z_{2h}). \quad (3)$$

The component of the wave function in the xy plane is taken as a product of the ground state wave functions for an electron (hole) in a 2D harmonic oscillator confinement potential, i.e.,

$$\psi_\perp(\boldsymbol{\rho}_{1e},\boldsymbol{\rho}_{2e},\boldsymbol{\rho}_{1h},\boldsymbol{\rho}_{2h}) = \phi(\boldsymbol{\rho}_{1e})\phi(\boldsymbol{\rho}_{2e})\phi(\boldsymbol{\rho}_{1h})\phi(\boldsymbol{\rho}_{2h}), \quad (4)$$

where

$$\phi(\boldsymbol{\rho}_{ij}) = \frac{1}{l_j\sqrt{\pi}}\exp\left(-\frac{1}{2l_j^2}\rho_{ij}^2\right), \quad (5)$$

$i=1, 2$ and $j=e, h$. Here, $l_j = \sqrt{\hbar/m_j^*\omega}$ is the length of the harmonic oscillator confinement and $\rho_{ij} = \sqrt{x_{ij}^2+y_{ij}^2}$. Averaging the Hamiltonian (1) over the ρ-component $\psi_\perp(\boldsymbol{\rho}_{1e},\boldsymbol{\rho}_{2e},\boldsymbol{\rho}_{1h},\boldsymbol{\rho}_{2h})$, we obtain the following effective 1D Hamiltonian:

$$H_{XX}^{eff} = -\frac{1}{2}\sum_i\left(\frac{\partial^2}{\partial z_{ie}^2} + \frac{1}{\sigma}\frac{\partial^2}{\partial z_{ih}^2}\right) + \sum_{ij\neq i'j'}U_{eff}(z_{ij}-z_{i'j'}), \quad (6)$$

where $\sigma = m_h/m_e$ is the mass ratio between the hole and the electron, and U_{eff} is the effective Coulomb potential obtained by averaging the real Coulomb potential over the wave function (4). It can be written as[24,25]

$$U_{eff}(z_{ij}-z_{i'j'}) = \gamma_{j'}^j\frac{\sqrt{\pi/2}}{l_{jj'}}\mathrm{erfcx}\left(\frac{|z_{ij}-z_{i'j'}|}{\sqrt{2}l_{jj'}}\right)(ij\neq i'j'), \quad (7)$$

where $i=1, 2$ and $j=e, h$, $\gamma_{j'}^j$ takes the values ±1, depending on the charges of the particles. In Eq. (7), $\mathrm{erfcx}(x) = \exp(x^2)\mathrm{erfc}(x)$ is the exponentially scaled complementary error function, and $\mathrm{erfc}(x) = 1 - \frac{2}{\sqrt{\pi}}\int_0^x dt\exp(-t^2)$ is the complementary error function, and

$$l_{jj'} = \begin{cases} l_j, & j=j', \\ \sqrt{(l_j^2+l_{j'}^2)/2}, & j\neq j'. \end{cases}$$

In Eq. (6), we adopt the donor Bohr radius $a_d = \varepsilon\hbar^2/m_e^*e^2$ and twice the donor Rydberg energy $2R_d = \hbar^2/m_e^*a_d^2$ as the units of length and the energy, respectively. For the effective 1D biexciton, the relative coordinates and the center-of-mass coordinates can be written as

$$z_{1e1h} = z_{1e} - z_{1h}, \quad z_{2e2h} = z_{2e} - z_{2h}, \quad (8)$$

$$Z_{1e1h} = \frac{1}{M}(m_e z_{1e} - m_h z_{1h}), \quad Z_{2e2h} = \frac{1}{M}(m_e z_{2e} - m_h z_{2h}), \quad (9)$$

$$z = Z_{1e1h} - Z_{2e2h}, \; Z = \frac{1}{2M}[m_e(z_{1e}-z_{2e}) + m_h(z_{1h}-z_{2h})], \quad (10)$$

where z_{1e1h}, z_{2e2h}, Z_{1e1h}, and Z_{2e2h} are the relative coordinates and the center-of-mass coordinates of the two excitons, respectively, and z and Z are the relative coordinate and the center-of-mass coordinate of the 1D biexciton, $M = m_e + m_h$ is the effective mass of the exciton. Then, Hamiltonian (6) can be written as follows:

$$H_{XX}^{eff} = H_{XX}^{rel} - \frac{1}{4M}\frac{\partial^2}{\partial Z^2}, \quad (11)$$

where

$$H_{XX}^{rel} = -\frac{1}{2\mu}\left(\frac{\partial^2}{\partial z_{1e1h}^2} + \frac{\partial^2}{\partial z_{2e2h}^2}\right) - \nu\frac{\partial^2}{\partial z^2} + \sum_{ij\neq i'j'}U_{eff}(z_{iji'j'}). \quad (12)$$

Here, $\mu = \sigma/(1+\sigma)$, $\nu = 1/(1+\sigma)$, and the inter particle distance along the wire can be written as

$$\begin{aligned} z_{1e2e} &= z + \mu(z_{1e1h} - z_{2e2h}), \\ z_{1h2h} &= z + \nu(z_{2e2h} - z_{1e1h}), \\ z_{1e2h} &= z + \mu z_{1e1h} + \nu z_{2e2h}, \\ z_{2e1h} &= -z + \nu z_{1e1h} + \mu z_{2e2h}. \end{aligned} \quad (13)$$

The z-component wave function $\phi_{||}$ can be separated into a product of the center mass and the relative wave function, i.e.,

$$\phi_{||} = \phi_{||}^{CM}(Z)\phi_{||}^{rel}(z_{1e1h}, z_{2e2h}, z). \quad (14)$$

We solve the relative Hamiltonian (12) by using the finite difference method on a three-dimensional uniform grid. We use 99 points in each of the z_{1e1h}, z_{2e2h}, and z directions. The energy E_{XX} and the wave function of the biexciton in a QWR then can be obtained. The binding energy of the biexciton can be calculated as $E_{BXX} = 2E_X - E_{XX}$, where E_X is the energy of a single exciton, which can be calculated by a similar method.

III. RESULTS AND DISCUSSIONS

Next, we discuss the properties of the biexciton. We present our results in two parts, Sec. III A for QWRs with identical electron and hole lateral confinement and Sec. III B for QWRs with different electron and hole lateral confinement.

A. Identical electron and hole lateral confinement

The binding energy and the structure of the biexciton have a close relationship with the Coulomb interactions between the particles in the biexciton. In our model, for equal electron and hole lateral confinement ($l_e = l_h = L$), the electron-electron, hole-hole, and electron-hole interactions have the same form. The conditional total interaction $\sum_{ij\neq i'j'} U_{eff}(z_{ij} - z_{i'j'})$ for zero exciton-exciton center-of-mass separation is plotted in Fig. 1(a) as a function of z_{e1h1} and z_{e2h2} for $L = 1$. The minimum values of the conditional interaction potential are along the lines $z_{1e1h} = 0$ and $z_{2e2h} = 0$ along which the electron and the hole of both individual excitons are in the same position under the condition of zero exciton-exciton center-of-mass separation. The conditional potential is maximal along the diagonal $z_{1e1h} = z_{2e2h}$, where the two particles of the same charge are localized at the same point along the wire length. The cross sections of the conditional interaction potential along the three straight lines in Fig. 1(a) are shown in Fig. 1(b) as functions of $z_{1e1h} - z_{2e2h}$. There is a potential well on the antidiagonal of the conditional interaction contours [cf. solid line in Fig. 1(b)], and it is broadly similar to that of Fig. 1(b) in Ref. 25 but with a deeper well potential.[25] The potentials along the paths plotted with dashed and dotted-dashed lines in Fig. 1(a) have the form of a double potential well with a barrier near the diagonal [cf. dashed and dotted-dashed lines in Fig. 1(b)]. Moving along the antidiagonal of Fig. 1(a) is equivalent to simultaneously interchanging the position the two identical particles in a biexciton with a zero exciton-exciton center-of-mass separation.

Fig. 2 shows contour plots of the conditional wave functions of the biexcitons calculated for different effective mass ratios for $L = 0.2$. In Fig. 2, plots (a)–(d) ((e)–(h)) are the conditional wave functions for the two electrons (two holes) in a biexciton with a fixed h–h (e–e) separation $\langle z_{hh}\rangle \approx 0.52a_d(\langle z_{ee}\rangle \approx 0.52a_d)$. From Figs. 2(a)–2(d), one can see that the two electrons have a probability distribution which is very similar to what is found in a molecular system, such as a H_2 molecule. The biexciton conditional wave function for $\sigma = 1$ is the same for both electrons and holes, which suggests that the electrons and holes are identical except for their opposite charges in the case of $\sigma = 1$. The cases $\sigma = 1.98$, 6.72, and 15.2 correspond to the material parameters of CdTe ($m_h = 0.19m_0$, $m_e = 0.096m_0$, $a_d = 5.4$ nm, and $2R_d = 27.6$ meV), GaAs ($m_h = 0.45m_0$, $m_e = 0.067m_0$, $a_d = 9.8$ nm, and $2R_d = 11.9$ meV), and InAs ($m_h = 0.41m_0$, $m_e = 0.027m_0$, $a_d = 29.7$ nm, and $2R_d = 3.2$ meV), respectively.[25] It is clear that as the value of σ increases, the electrons become more tightly bound to the holes. The heavier the hole effective mass is, the more difficult it is for the holes to move in the biexciton.

In the following discussion, we will see that the electron and hole in the biexciton have a tendency to stay close to each other, and the e–h PCFs have a high probability at zero e–h distance. Therefore, the larger the mass ratio is, the more tightly bound are the electrons and holes in the biexciton. Moreover, the local minimum along the diagonal in Figs. 2(e)–2(h) becomes more pronounced as σ increases. The evolution of the wave function with σ is related to the tunneling of the particles of the same charge through the potential barrier shown in Fig. 1(b). The electrons in the biexciton, with light effective masses, tunnel easily through the diagonal barrier due to the inter-electron repulsion. On the other hand, the diagonal barrier is effectively much larger for the heavy-mass holes which prevents them penetrating the barrier at large σ.

In Fig. 3(a), we plot the biexciton binding energies as functions of the lateral confinement length for $\sigma = 1.98$, 6.72, and 15.2. From Fig. 3(a), one can see that the biexciton binding energies decrease with increasing confinement length for different values of σ. As the confinement length decreases, the spatial confinement gets stronger, and the increased spatial confinement shrinks the biexciton in the longitudinal direction. Therefore, all of the particles in the biexciton get closer to each other, which explains the increase in the binding energy as the lateral confinement length decreases. Fig. 4(b) shows the biexciton binding energy versus the mass ratio σ for $L = 0.2$. An increase in the mass ratio clearly increases the biexciton binding energy.

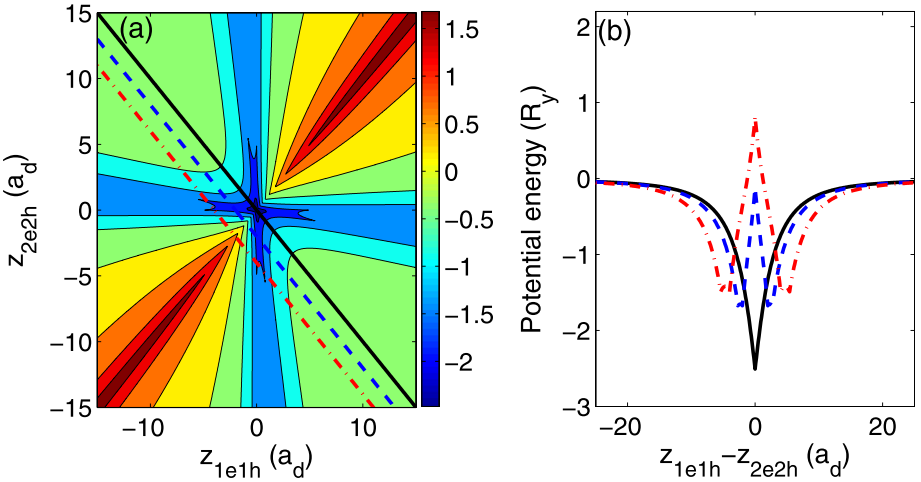

FIG. 1. (a) Contour plot of the conditional total Coulomb interaction potential $V = U_{eff}(L, z_{1e2e}) + U_{eff}(L, z_{1h2h}) - U_{eff}(L, z_{1e1h}) - U_{eff}(L, z_{1e2h}) - U_{eff}(L, z_{1h2e}) - U_{eff}(L, z_{2e2h})$ for $z = 0$ as a function of the interparticle distances with lateral confinement length $L = l_e = l_h = 1$. (b) The interaction potential plotted for $L = 1$ along the lines $z_{2e2h} = -z_{1e1h}$, $z_{2e2h} = -z_{1e1h} - 2$, and $z_{2e2h} = -z_{1e1h} - 4$ marked in (a) with solid, dashed, and dotted-dashed lines, respectively, as a function of $z_{e1h1} - z_{e2h2}$. Distances and energies are given in donor units.

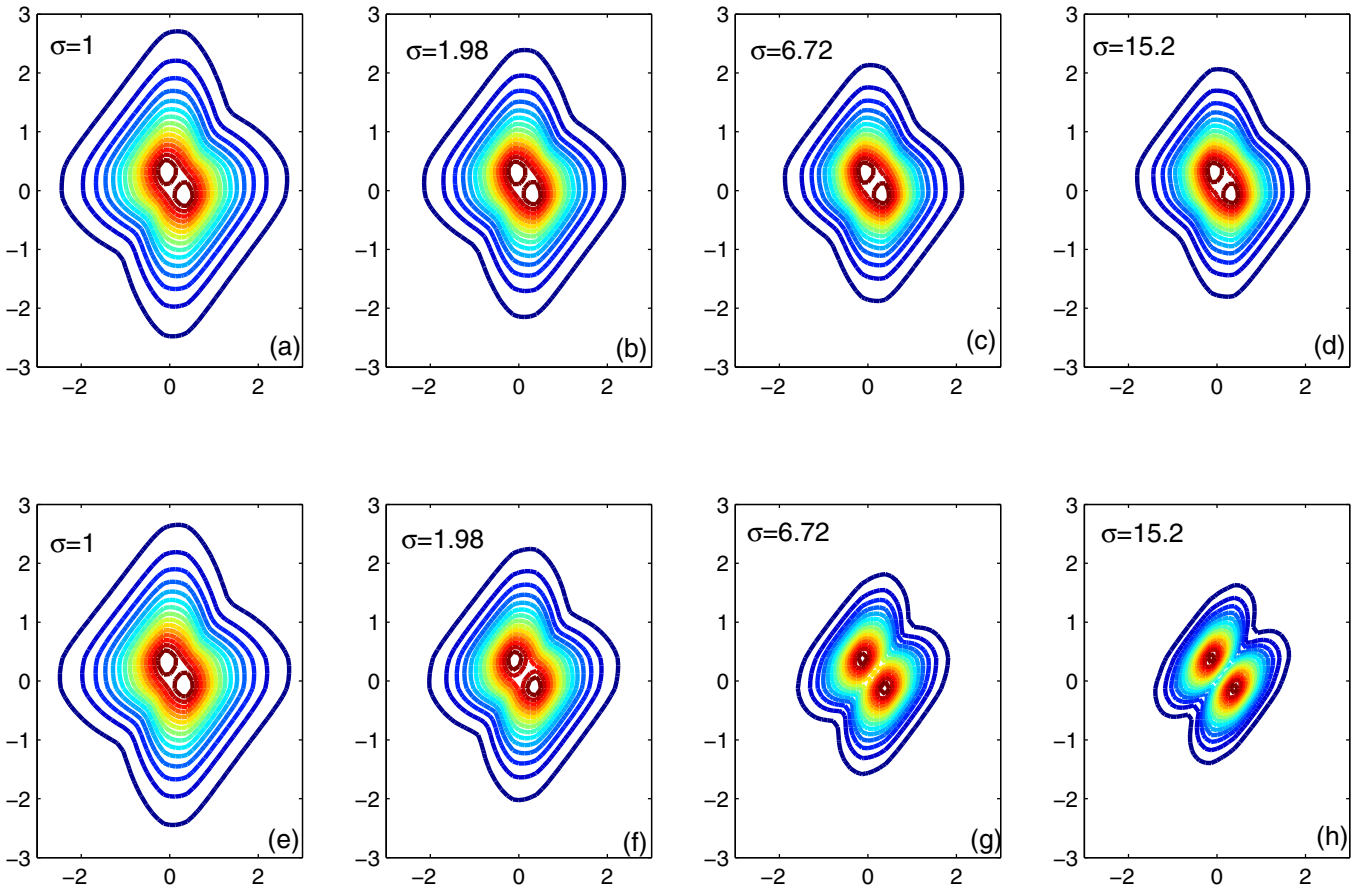

FIG. 2. Contour plots of the conditional biexciton wave functions with a fixed hole position $\langle z_{hh}\rangle \approx 0.52a_d$ ((a)–(d)) and with a electron fixed position $\langle z_{ee}\rangle \approx 0.52a_d$ ((e)–(h)) for $L = 0.2$ in z_{1e1h} and z_{2e2h} coordinates for different values of the mass ratio σ.

The average interparticle distance can give a clear picture of the structure of the biexciton. In Fig. 4(a), we plot the average distance between the two electrons, between the two holes, and between the electron and hole as function of the lateral confinement length. The average distances are defined as

$$\langle z_{ij}\rangle = \int |\phi_{\|}(z_{1e}, z_{2e}, z_{1h}, z_h)|^2 |z_i - z_j| dz_{1e} dz_{2e} dz_{1h} dz_h, \quad (15)$$

with $i, j = 1e, 2e, 1h, 2h$. The σ dependence of the average distances between the particles in the biexciton is shown in Fig. 4(b). The size of the biexciton increases with increasing lateral confinement length. In order to get a state of minimum energy, the distance between the particles of different charges is expected to be smaller than that between the

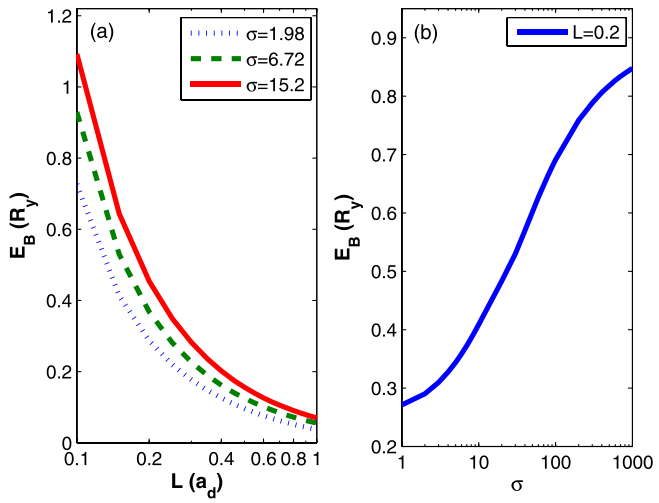

FIG. 3. (a) The biexciton binding energies as functions of the lateral confinement length for different values of the mass ratio σ. (b) The biexciton binding energies as functions of the values of σ for lateral confinement length $L = 0.2$. Energies and lengths are in donor units.

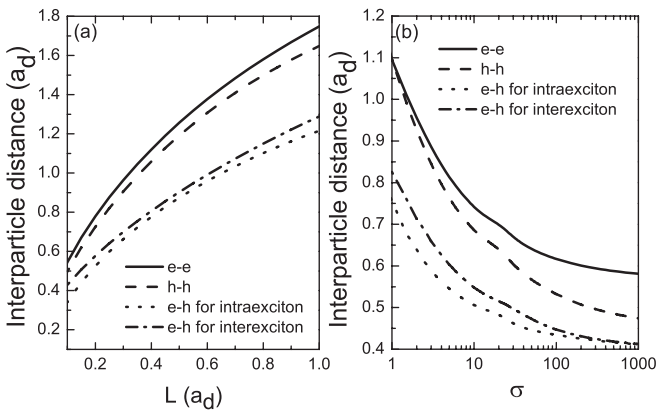

FIG. 4. The average interparticle distances for a biexciton as functions of (a) the lateral confinement lengths for $\sigma = 6.72$ and (b) the mass ratio σ for $L = 0.2$. Here, e–e, e–h and h–h stand for the electron-electron, the electron-hole and the hole-hole distances.

particles with identical charges, and this can be seen in Figs. 4(a) and 4(b). The average e–e distance is slightly larger than the average h–h distances indicating that the e–e correlation distance is larger than that for h–h. A similar phenomenon can be seen in the average interexciton and intraexciton e–h distances. Energetically, the most favored configuration in a 1D system is e–h–e–h or h–e–h–e, which means that no two identical particles in the biexciton are physically contiguous. The average e–h distances for the interexciton and for intraexciton cases represent the distances between nearest-neighbor particles and the distance between the two extreme particles in the above configuration. A slightly larger average interexciton e–h distance suggest that individual excitons may retain their identity in bound biexcitons. The σ dependence of the average interparticle distances in the biexciton is shown in Fig. 4(b). The average distance $\langle z_{ij}\rangle$ decreases with decreasing σ. It is interesting to note that the average e–e distance and the h–h distance are different in the hydrogenic limit ($1/\sigma \to 0$) and gradually tend to the same value in the positronium limit ($\sigma = 1$). While the average e–h distance for the intraexciton and for interexciton cases are different for equal electron and hole masses, they gradually tend to the same value in the hydrogenic limit. It should be noted that the non smooth structures near $\sigma = 20$ in Fig. 4(b) are greatly magnified by the logarithmic coordinates and are nearly invisible if a linear scale is used.

The PCF of particles in a biexciton may reveal important information about the physics of biexciton binding. The PCF for the electron-hole pair is defined as

$$P_{eh}(z) = \frac{1}{2}\sum_{i=1e,2e}\sum_{j=1h,2h}\langle\delta(|z_i - z_j| - z)\rangle, \qquad (16)$$

and the PCF for the electron-electron (hole-hole) pair can be calculated as

$$P_{ee(hh)}(z) = \frac{1}{2}\sum_{\substack{i=1e,2e\\(1h,2h)}}\sum_{\substack{j=1e,2e\\(1h,2h)}}\langle\delta(|z_i - z_j| - z)\rangle. \qquad (17)$$

These functions are plotted in Fig. 5. Figs. 5(a)–5(c) show the e–h, e–e, and h–h PCF, respectively, for different confinement lengths. Fig. 5(d) shows the three PCFs for $L = 0.2$. In Fig. 5(a), one can see that the e–h PCF has its maximum value when the distance between the particles is zero, which means that the electrons and holes in the biexciton have a tendency to stay close to each other. For strong lateral confinement ($L = 0.2$), the e–h PCF exhibits a larger peak at zero interparticle separation and decays more rapidly with interparticle distance than in the other two cases. The e–e PCF [cf. Fig. 6(b)] has a considerable value at zero interparticle distance and peaks at a nonzero interparticle distance. It then decreases rapidly with increasing interparticle distance. For $L = 0.2$, the e–e PCF is negligible for interparticle distances larger than $3a_d$ and peaks at $z = 0.5a_d$. This indicates that the electrons in a biexciton can get close to each other and even have a significant probability at zero interparticle distance. The most popular configuration for two electrons is, however, to stay a certain distance away from each other

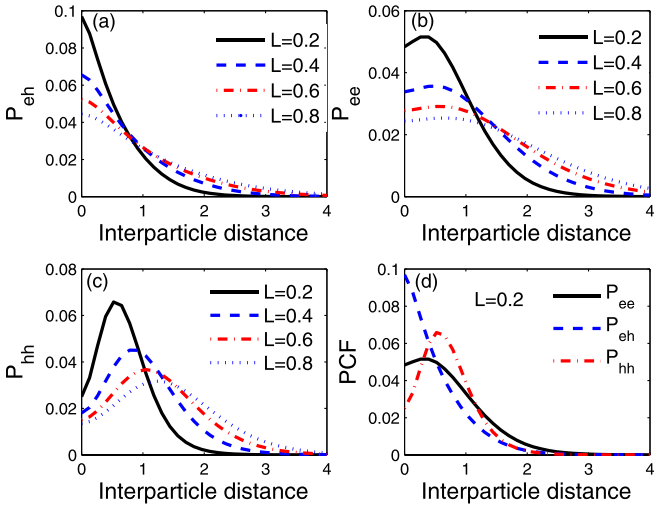

FIG. 5. Electron-hole (a), electron-electron (b), hole-hole (c) pair correlation functions plots for biexciton in different QWRs. Plot (d) displays a comparison between the three PCFs for $L = 0.2$. Lengths are in donor units.

as a consequence of the Coulomb repulsion. The h–h PCF [cf. Fig. 5(c)] is peaked at a finite distance and decays faster for the strong lateral confinement ($L = 0.2$). It is similar to the e–e case but with a smaller value at zero interparticle distance. The reason is that it is more difficult for the heavier holes in the biexciton to tunnel through the potential barrier and have a significant probability of being at zero interparticle distance. The longer tail in the e–e PCF [cf. Fig. 5(d)] indicates that the electrons are more extended and are still correlated even at large distances, which suggests that the size of the biexciton should be judged by examining the e–e PCF. This is confirmed by Fig. 4. In summary, the picture for the particle configuration in a biexciton is that the electrons and holes orbit around each other as in single excitons and that the centers of mass of the two excitons are separated by a certain distance.

Since the total interaction potential $U_{total} = \sum_{ij\neq i'j'} U_{eff}(z_{ij} - z_{i'j'})$ dominates the properties of the biexciton in QWRs, we plot its expectation value $\langle U_{total}\rangle$ as a function of the exciton-exciton center-of-mass separation z in Fig. 6.

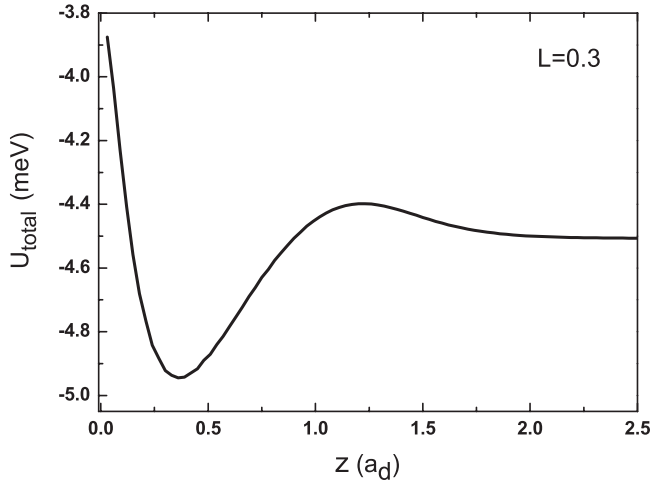

FIG. 6. The total interaction potential U_{total} as a function the exciton center-of-mass separation z for confinement length $L = 0.3a_d$.

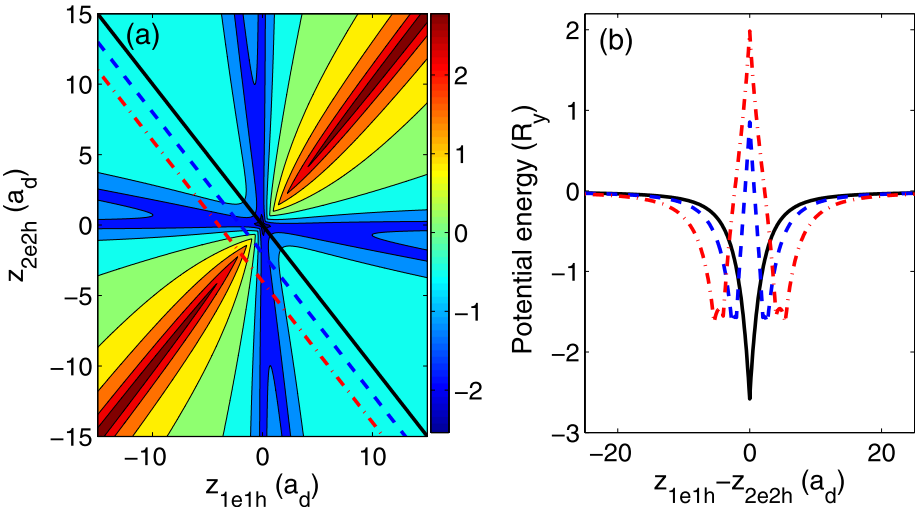

FIG. 7. Same as Fig. 1 but for different electron and hole lateral confinement lengths $l_e = 1$ and $l_h = 0.5$. Distances and energies are given in donor units.

From Fig. 6, one can see that when $z \leq 1.25a_d$, $\langle U_{total} \rangle$ decreases rapidly at first as z increases, until it reaches a minimum and then gradually increases. When $z > 1.25a_d$, however, it decays slowly again as z increases.

B. Different electron and hole lateral confinement

In this section, we focus on the effects on the properties of biexcitons in QWRs of having different electron and hole lateral confinement.

Fig. 7 is the same as Fig. 1 but for unequal lateral confinement lengths $l_e = 1$ and $l_h = 0.5$. The potential maximum values along the diagonal $z_{1e1h} = z_{2e2h}$ and the minimum values along $z_{1e1h} = 0$ and $z_{1e1h} = 0$ in Fig. 7(a) are both strengthened with respect to that in Fig. 1, as can be clearly seen in Fig. 7(b). The reason is that a stronger hole confinement increases both the hole-hole repulsive interaction and the electron-hole attractive interaction.

The effect of hole confinement on the biexciton binding energies is plotted in Fig. 8. From Fig. 8, one can see that the biexciton binding energy increases gradually as the hole confinement length l_h increases, until it reaches a maximum and then slowly decreases. In the biexciton system, the increased hole confinement length decreases both the h–h repulsive interaction and the e–h attractive interaction, and there are two opposite effects on the stability of biexciton: The decreased h–h interaction stabilizes the system and increases the binding energy, while the decreased e–h interaction destabilizes the system. It is the two competing trends that induce a non-monotonic functional relationship between the biexciton binding energies and the hole confinement length.

Experimentally, the biexciton binding energies are measured to be 1.2 meV and 1.5 meV for V-shaped GaAs/AlGaAs quantum wires having a GaAs crescent thickness of 7.1 nm and 5 nm, respectively, at the center.[1,4,5] The calculated biexciton binding energy was fitted to the experimental value of 1.5 meV using $l_e = 5.0$ nm and $l_h = 4.9$ nm. For $l_e = 7.1$ nm, the maximum calculated biexciton binding energy is 1.12 meV at $l_h = 4.4$ nm, which is slightly smaller than the experimental value 1.2 meV. A possible reason for the discrepancy may be that interfacial disorder in the

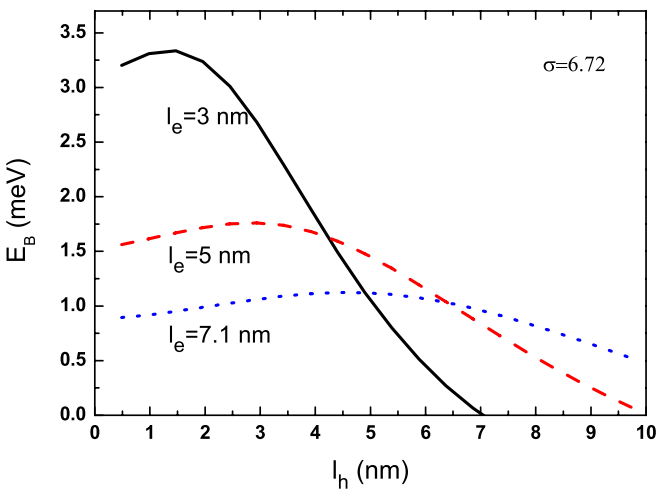

FIG. 8. Biexciton binding energy as a function of the hole confinement length for GaAs material parameters and electron confinement lengths $l_e = 3$ nm, 5 nm, and 7.1 nm.

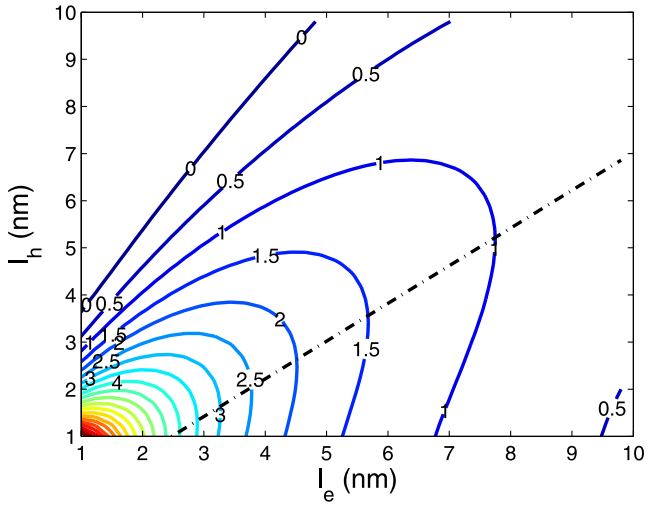

FIG. 9. Contour plots depicting the biexciton binding energies as a function of the electron and hole confinement lengths for GaAs material parameters. Each contour line represents a value for the binding energy (in units of meV) of the biexciton in QWR. The dash dot line, parametrized by $l_h = 0.8l_e - 0.98$ nm, shows the path along which the biexciton has the maximum binding energy.

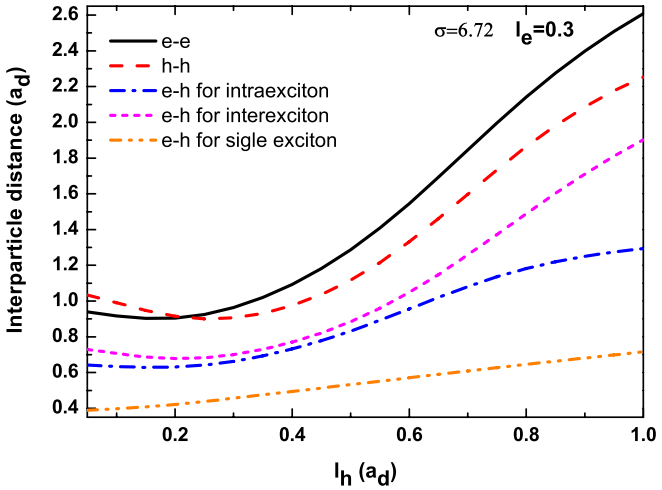

FIG. 10. The average interparticle distance of the biexciton versus the hole confinement length for the case of GaAs material parameters and $l_e = 0.3a_d$. Here, e–e, e–h, and h–h stand for the electron-electron, the electron-hole, and the hole-hole distances.

experimental sample increases the binding energy of the biexciton.[8,28]

Fig. 9 depicts contours for the binding energy of the biexciton in QWRs in the $l_e - l_h$ plane. The maximum of the biexciton binding energy presented in Fig. 8 follows a path that is nearly linear for $l_e > 2.45$ nm and is approximately parametrized by $l_h = 0.8l_e - 0.98$ nm. The biexciton binding energy in the long-l_h-short-l_e (upper left) region becomes negative, and the biexcitons in this region are unbound. In the short-l_h-short-l_e region (lower left), the contour lines become quite dense, which indicates that the binding energies of the biexcitons in this region are sensitively dependent on the lateral confinement strength.

The average interparticle distances in the biexciton as functions of the hole confinement length are shown in Fig. 10 for GaAs material parameters and $l_e = 0.3a_d$. It is found that the size of the biexciton and the exciton show different behaviour as l_h increases. With increasing hole confinement, the size of the exciton increases monotonically due to the reduced value of the electron-hole interaction, while the size of the biexciton decreases slowly at first and then increases rapidly. This is also a consequence of competition between the decreased *h–h* repulsive interaction and the decreased *e–h* attractive interaction. We may also note that the difference between the electron-hole distance for the interexciton and intraexciton cases gets large when $l_h > 0.7$ a_d, which implies that the biexciton becomes unbound as can be confirmed by Fig. 8.

IV. CONCLUSIONS

In summary, we have studied, using the finite difference method, the properties of biexcitons in quantum wires with strong lateral confinement. The binding energy, conditional wave function, average interparticle distance, the total interaction potential, and the pair correlation function of biexcitons in QWRs have been investigated theoretically. The calculated biexciton binding energies have been compared with experimental measurements, and a reasonable result has been obtained. The biexciton conditional wave function shows that the biexciton structure is similar to that of the H_2 molecule. The difference between the average electron-hole distance for the interexciton and intraexciton cases suggest that the excitons in bound biexcitons may retain their identity. The effects of different electron and hole lateral confinement on the properties of biexcitons in QWRs have also been investigated.

ACKNOWLEDGMENTS

This work was supported by the Natural Science Foundation of Hebei Province (Grant Nos. A2013205102 and A2011205092), the Science and Technology Research and Development Program of Hebei Province (Grant No. 11215179), and the Natural Science Research Project of Education Department of Hebei province (Grant No. Q2012017). The authors would like to thank Professor N. E. Davison for his helpful suggestions.

[1]X. L. Wang, M. Ogura, and H. Matsuhata, Appl. Phy. Lett. **67**, 3629 (1995).
[2]L. Bányai, I. Galbraith, C. Ell, and H. Haug, Phys. Rev. B **36**, 6099 (1987).
[3]A. Balandin and S. Bandyopadhyay, Phys. Rev. B **54**, 5712 (1996).
[4]A. Crottini, J. L. Staehli, B. Deveaud, X. L. Wang, and M. Ogura, Solid State Commun. **121**, 401 (2002).
[5]T. Guillet, R. Grousson, V. Voliotis, M. Menant, X. L. Wang, and M. Ogura, Phys. Rev. B **67**, 235324 (2003).
[6]T. Baars, W. Braun, M. Bayer, and A. Forchel, Phys. Rev. B **58**, R1750 (1998).
[7]Y. Hayamizu, M. Yoshita, Y. Takahashi, H. Akiyama, C. Z. Ning, L. N. Pfeiffer, and K. W. West, Phys. Rev. Lett. **99**, 167403 (2007).
[8]A. Feltrin, F. Michelini, J. L. Staehli, B. Deveaud, V. Savona, J. Toquant, X. L. Wang, and M. Ogura, Phys. Rev. Lett. **95**, 177404 (2005).
[9]R. C. Miller, D. A. Kleinman, A. C. Gossard, and O. Munteanu, Phys. Rev. B **25**, 6545 (1982).
[10]J. Singh, D. Birkedal, V. G. Lyssenko, and J. M. Hvam, Phys. Rev. B **53**, 15909 (1996).
[11]A. V. Filinov, C. Riva, F. M. Peeters, Yu. E. Lozovik, and M. Bonitz, Phys. Rev. B **70**, 035323 (2004).
[12]Z. P. Wang and X. X. Liang, Solid State Commun. **150**, 356 (2010).
[13]R. M. Lee, N. D. Drummond, and R. J. Needs, Phys. Rev. B **79**, 125308 (2009).
[14]J. Usukura, Y. Suzuki, and K. Varga, Phys. Rev. B **59**, 5652 (1999).
[15]M. Ikezawa, S. V. Nair, H. W. Ren, Y. Masumoto, and H. Ruda, Phys. Rev. B **73**, 125321 (2006).
[16]T. F. Rønnow, T. G. Pedersen, and B. Partoens, Phys. Rev. B **85**, 045412 (2012).
[17]D. Birkedal, J. Singh, V. G. Lyssenko, J. Erland, and J. M. Hvam, Phys. Rev. Lett. **76**, 672 (1996).
[18]Y. Masumoto, S. Yoshida, M. Ikezawa, S. Tomimoto, and Y. Sakuma, Appl. Phy. Lett. **98**, 061905 (2011).
[19]S. Amloy, K. H. Yu, K. F. Karlsson, R. Farivar, T. G. Andersson, and P. O. Holtz, Appl. Phy. Lett. **99**, 251903 (2011).
[20]M. E. Reimer *et al.*, Nano Lett. **11**, 645 (2011).
[21]X. Li *et al.*, Science **301**, 809 (2003).
[22]K. Edamatsu, G. Oohata, R. Shimizu, and T. Itoh, Nature (London) **431**, 167 (2004).
[23]R. Johne, N. A Gippius, G. Pavlovic, D. D. Solnyshkov, I. A. Shelykh, and G. Malpuech, Phys. Rev. Lett. **100**, 240404 (2008).
[24]S. Bednarek, B. Szafran, T. Chwiej, and J. Adamowski, Phys. Rev. B **68**, 045328 (2003).
[25]B. Szafran, T. Chwiej, F. M. Peeters, S. Bednarek, and J. Adamowski, Phys. Rev. B **71**, 235305 (2005).
[26]Y. Sidor, B. Partoens, and F. M. Peeters, Phys. Rev. B **71**, 165323 (2005).
[27]Y. Sidor, B. Partoens, and F. M. Peeters, Phys. Rev. B **77**, 205413 (2008).
[28]O. Mayrock, H.-J. Wünsche, F. Henneberger, C. Riva, V. A. Schweigert, and F. M. Peeters, Phys. Rev. B **60**, 5582 (1999).